Journal of
Applied
Crystallography
ISSN 0021-8898

Received 3 June 2009
Accepted 16 September 2009

Design challenges and performance of nested neutron mirrors for microfocusing on SNAP

Gene E. Ice,[a]* Judy W. L. Pang,[a] Chris Tulk,[b] Jamie Molaison,[b] Jae-Young Choi,[c] Cody Vaughn,[d] Lauren Lytle,[d] Peter Z. Takacs,[e] Ken H. Andersen,[f] Terry Bigault[f] and Ali Khounsary[g]

[a]MST Division, Oak Ridge National Laboratory, TN 37831-6118, USA, [b]Spallation Neutron Source, Oak Ridge National Laboratory, TN 37831-6459, USA, [c]Pohang Accelerator Laboratory, Pohang, Republic of Korea, [d]Governors Academy, University of Tennessee–Knoxville, Tennessee, USA, [e]Instrumentation Division, Brookhaven National Laboratory, Upton, NY 11973, USA, [f]Institut Laue–Langevin, Grenoble, France, and [g]Advanced Photon Source, Argonne National Laboratory, IL 60439, USA. Correspondence e-mail: icege@ornl.gov

Kirkpatrick–Baez (KB) neutron supermirrors can efficiently focus polychromatic neutron beams to micrometre dimensions. The ultimate size is determined mainly by the perfection of the mirrors and by the size of the beam needed to have sufficient experimental signal. Nested or Montel KB mirrors can collect ~2.6 times more beam than standard sequential KB optics, but require good figure perfection at the edge of one mirror. This paper describes the characterization of the figure errors over the important reflective portions of the two mirrors needed for a Montel focusing pair. The measurements are placed in context with theoretical predictions and are used to predict mirror focusing performance. Strategies to improve on the focusing of this class of optics are suggested and early results from these mirrors installed on the Spallation Neutrons at Pressure (SNAP) Beamline 3 at the Spallation Neutron Source (SNS) at Oak Ridge are presented.

1. Introduction

Achromatic focusing optics are essential for many classes of neutron instruments because they can greatly improve the signal-to-noise ratio, S/N, for experiments on small (<1 mm) samples. Over the past three decades, X-ray optics have rapidly improved, driven by the emergence of powerful synchrotron sources (Liu *et al.*, 2005; Ice, 2007). Achromatic micro- and nanobeam X-ray mirror optics have made particularly impressive gains in spatial resolution and can now produce the smallest hard X-ray beams (Mimura *et al.*, 2007). With the recent development of spallation neutron sources of unprecedented brightness, these same focusing ideas have recently been applied to neutron beams (Ice *et al.*, 2005, 2006; Ice, 2008). For example, the Spallation Neutron Source (SNS) at Oak Ridge has set a new world record for neutron brilliance from a pulsed source, enabling many new experiments; it routinely runs at ~500 kW and is progressing towards a goal of 1.4 MW (NanoTechWire.com, 2009). One particularly important advantage of the SNS is its ability to study smaller sample volumes. For small-sample experiments on a spallation source, achromatic focusing is especially important since neutron energy is encoded by time-of-flight, and broad-bandpass experiments use the available neutron flux more efficiently.

Traditional neutron optics based on beam guides and beam-defining apertures provide a flux that scales with the beam size squared for large beams, but with the beam size to the fourth power for small beams (Ice *et al.*, 2005). For thermal neutrons, the crossover between when it is best to use a beam guide with an aperture and when it is best to use an imaging system is for beams of about 1–2 mm, depending on the clearance between the last optical element and the sample (Ice *et al.*, 2005). For beams of less than ~1 mm, focusing optics provide a higher intensity at the sample and the beam flux scales with the probe size squared. This difference between the intensity in a small beam formed by an aperture on a conventional neutron beamline and the intensity in a focused beam formed with imaging optics is due to the need to collimate a conventional beam to keep it from spreading over the typical drift distance between the last optical element in the beamline and the sample position. This distance is needed for environmental chambers, detectors and other instrumentation and is typically 0.1–0.25 m.

A demonstration experiment using a traditional Kirkpatrick–Baez (KB) mirror system (Kirkpatrick & Baez, 1948) was carried out at Chalk River (Ice *et al.*, 2006). This demonstration confirmed that KB optics efficiently preserve source brilliance at the sample. However, KB optics are limited by the total divergence that can be focused onto the sample; if θ_{max} is the maximum incidence angle for efficient reflection of a wavelength λ from a supermirror, then traditional KB optics can collect a divergence of about $0.84\theta_{max}$

onto the sample in each direction. θ_{max} is usually defined as the inflection point in the reflectivity curve as a function of the glancing angle θ, and is usually a sharp cutoff. Supermirrors provide a way to increase the focused divergence; a supermirror is characterized by its reflectivity and m number, which describes the ratio between the angle for efficiently reflecting neutrons of wavelength λ and the maximum angle for efficient reflection from a nickel mirror. Natural Ni mirrors efficiently reflect neutrons as long as $\sin\theta < 0.217\lambda/4\pi$, where λ is in nm and 0.217 has units of nm^{-1} (see, for example, SwissNeutronics, 2009; http://www.swissneutronics.ch/products/concept-supermirrors.html). Therefore, for a supermirror the maximum angle for efficient reflecting, θ_{max}, is proportional to the wavelength and m, and is given in radians by

$$\theta_{max} = m\lambda/57.9. \quad (1)$$

One way to increase the limited convergence that can be collected onto the sample by sequential KB mirrors is through the use of nested or Montel mirrors (Fig. 1). This variant of KB optics can collect about $1.34\theta_{max}$ in each direction and can therefore focus about 2.6 times more intensity onto the sample than with a standard sequential KB system. However, in order for the system to work near its theoretical limit, the beam must efficiently reflect near the edge of one of the mirrors (Figs. 1 and 2) (Ice, 2008). In addition, the larger numerical aperture of nested optics makes it more important to use nearly perfect elliptical surfaces to avoid figure-error-induced aberrations. The need for nested mirrors to operate near the edge of at least one mirror can introduce several errors: mirror round-off from polishing, oxidation of the mirror surface near the mirror edge, mirror delamination along the edge and local anticlastic bending in bent mirrors (Yang *et al.*, 2003). Here, we have characterized the mirror surface at the edge of a mirror from our nested KB mirror pair and compared its surface figure with that at the mirror center. The measurements were made with a special long-trace profiler (LTP) (Puzyrev *et al.*, 2009) that can easily characterize the mirror figure in both vertical and horizontal deflecting orientations. This information is essential to determine the performance limits of the mirror pair.

2. Mirror figuring approach

The mirrors used for the nested Spallation Neutrons at Pressure (SNAP) optics at the SNS are deposited on specially polished quartz substrates. The substrates were polished on all four sides, and were polished to minimize round-off errors at the edges. The Ni–Ti supermirror coatings were deposited at the Institute Laue–Langevin (ILL), France (Ice *et al.*, 2009). Because the mirrors are designed to collect a very large divergence onto the sample, the focal length is roughly four times smaller at the downstream edge of the mirror than at the upstream edge. As a consequence, there is a large change in the ideal curvature along the mirror. Although the mirror figure could in principle be polished into a monolithic substrate, with the SNAP mirrors the curvature was controlled by bending the polished flat substrates.

Bent flat mirrors have been used for decades to produce high-performance elliptical surfaces for X-ray focusing. In general, bending is easy as long as the ratio of mirror length to image distance is small. However, when the mirror length to image distance ratio exceeds unity – as with the SNAP mirrors – then simple bending schemes based on asymmetric moments are no longer acceptable, and the mirror cross section is typically shaped to bend more accurately to the desired elliptical shape. With the SNAP mirrors, however, the mirror cross section is fixed, so a strategy that works without changing the mirror cross section is needed. As illustrated in Fig. 3(*a*), the required bending moment of the SNAP mirrors is highly nonlinear. The linear portion of the bending moment can be applied with unequal moments at the ends of the mirrors (Figs. 3*b* and 3*c*) The applied moment can be segmented into parts of unequal slope by the application of a force on the mirror between the mirror ends (Fig. 3*d*). Therefore, each mirror had three degrees of freedom for bending: independent bending moments applied to the ends and a spring-loaded force applied near the middle of the mirror. The applied moments at each end of the mirror were controlled by simple levers.

Once the mirrors were bent to the required elliptical shape, they were assembled on an alignment stage and brought together with a micrometer-driven linear stage. The mirrors were aligned perpendicular to each other by observing the interference pattern of a laser reflected at the corner where the two mirrors touched. As shown in Fig. 2, the system is

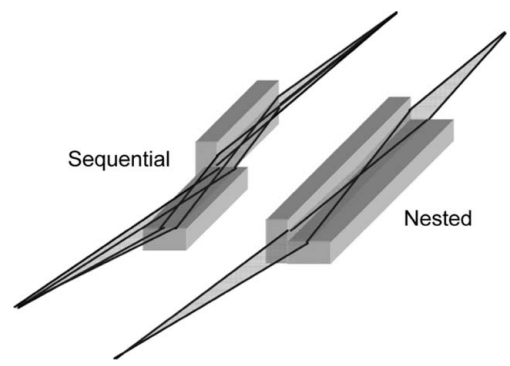

Figure 1
Sequential and nested KB mirrors.

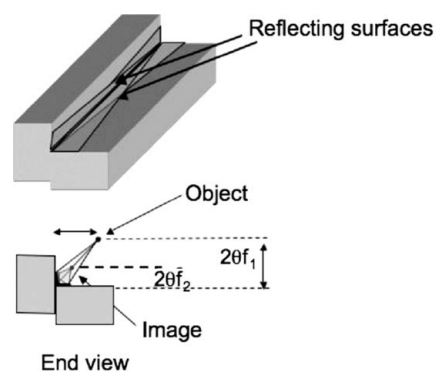

Figure 2
Two elliptical mirrors assembled so that the neutrons reflect off the corner between them.

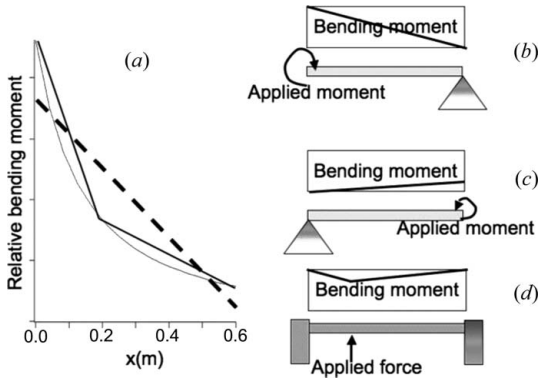

Figure 3
(*a*) The relative bending moment (gray line) required to bend a 0.6 m-long beam of uniform cross section into an ellipse with $f_1 \simeq 0.65$ and $f_2 \simeq 0.5$ m, compared with a best-approximation linear moment (dashed line) and a best approximation made up of two linear sections (segmented line). (*b*) A moment applied on the left end of a mirror creates a bending moment along the mirror that is a maximum on the left end of the mirror and goes to zero on the right end. (*c*) A moment applied on the right end of the mirror is maximum on the right end and goes to zero on the left end. (*d*) A force applied between the ends of a mirror that is fixed at each end creates moments along the mirror that are maximum under the force and go linearly to zero at the ends.

designed to reflect neutrons off both mirrors, but some neutrons reflect first off the horizontally focusing mirror and others reflect first off the vertically focusing mirror. In our approach, the mirrors are assembled so that the center of one mirror and the edge of the other are used (see Fig. 2, end view). Because the edges of these mirrors were not cut to an elliptical shape, there is a small gap between the two mirrors at the center of the assembly. This gap represents an ~20% loss of flux and contributes to a non-monotonic angular distribution in the focused beam. The losses and complicated divergence distribution of the beam can be greatly improved by cutting or polishing the edge of one mirror to match the elliptical curvature of its partner mirror. This approach will be pursued now that the performance of this prototype system has been confirmed. The slightly more complicated bending should be easy to compensate for by properly positioning and adjusting the force-applying spring.

2.1. Theory

When calculating blurring for nested KB mirrors, it is important to look at figure errors both in the scattering plane and perpendicular to it. These errors are typically referred to as in-plane, meridional or tangential errors, and out-of-plane or sagittal errors. The two kinds of errors are shown in Fig. 4. As illustrated, in-plane slope errors deflect the beam in the scattering plane defined by the incident beam and the ideal reflected beam. Out-of-plane errors deflect the beam perpendicularly to the scattering plane.

Meridional figure errors are almost always more important than sagittal figure errors for sequential KB mirrors, but may be similar in magnitude for nested pairs. For meridional focusing, the equation for blurring is

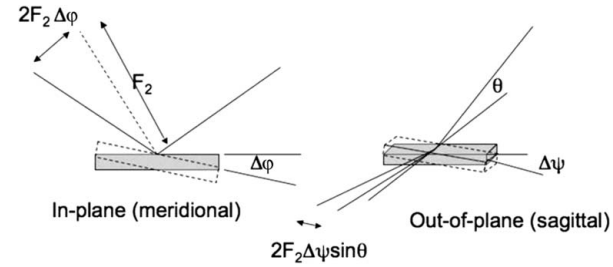

Figure 4
In-plane (tangential) and out-of-plane (sagittal) figure errors.

$$\Delta h_{\rm M} = 2F_2\Delta\varphi, \qquad (2)$$

where $\Delta h_{\rm M}$ is the blur of the focal spot in the scattering plane due to in-plane or meridional figure errors $\Delta\varphi$, with an image distance F_2. Out of the scattering plane, the image is blurred by $\Delta h_{\rm S}$, which is proportional not only to the image distance F_2 and the magnitude of the sagittal figure error $\Delta\psi$, but also to the sine of the glancing angle θ:

$$\Delta h_{\rm S} = 2F_2\Delta\psi\sin\theta. \qquad (3)$$

2.2. Mirror measurements

The mirror figure and slope errors were measured with the LTP. The software of the profiler calculates the r.m.s. deviations from an ideal ellipse, the parameters of which can be set in the program. For our nested mirrors, sagittal figure errors were estimated by measuring the slopes of the bent neutron mirrors perpendicular to their focusing plane (Fig. 5). Almost all of the slope changes are concentrated near the mirror edges. The worst peak-to-peak errors are of the order of 20 mrad and the average errors for the edge used are <10 mrad. With equation (3) and for a glancing angle of 4 mrad, an image distance of 0.5 m and r.m.s. sagittal errors of 10 mrad, the estimated r.m.s blurring of the image is ~14 μm.

The in-plane meridional figure was measured along the beam direction. Measurements were made both at the centers of the mirrors and near their edges. The r.m.s. slope errors could be adjusted to about 20 μrad. The deflection errors from

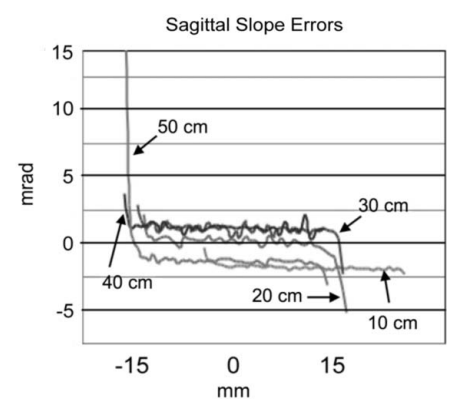

Figure 5
Slope measurements perpendicular to the scattering plane at 10 cm intervals along a bent neutron mirror.

Table 1
Measured mirror parameters.

The mirrors were fitted with the same object distance F_1, image distance F_2 and glancing angle θ.

	F_1 (m)	F_2 (m)	θ (rad)	R (m)	$\sigma_{\rm sagittal}$ (mrad)	$\sigma_{\rm meridional}$ (μrad)
Horizontally deflecting mirror	6.49	0.51	0.004	236	<1	20
Vertically deflecting mirror	6.49	0.51	0.004	236	<5	17

along the beam are estimated in Fig. 6. Slightly better slope errors were found with a slightly larger image distance (0.86 m), where the differences in the curvature at the front and back of the mirror are not as extreme. However, the larger image distance reduces the total flux that can be collected onto the sample and in general it is advantageous to have the focusing optics as close to the sample as possible without interfering with environmental chambers and detectors. Efforts are underway to improve the bending mechanism to achieve at least a factor of two better figure control with 0.5 m image distance. Table 1 summarizes the parameters measured for each mirror.

The estimated focal spot size was calculated by geometric ray tracing through a model nested KB mirror system. The object distance (6.49 m) and image distance (0.51 m) were set to the design goal of the SNAP beamline. Blurring from the slope errors was estimated by adding the ray-tracing and figure errors in quadrature (*i.e.* assuming Gaussian errors). The vertical spot size is determined from both the geometric model spot size and the measured in-plane slope errors of the vertically deflecting mirror. The horizontal spot size is determined by the geometric model spot size, the in-plane figure errors of the horizontally deflecting mirror and the out-of-plane (sagittal) slope errors of the vertically deflecting mirror (edge round-off). The estimated beam size is plotted in Fig. 7 as a function of object size and compared with the experimental results.

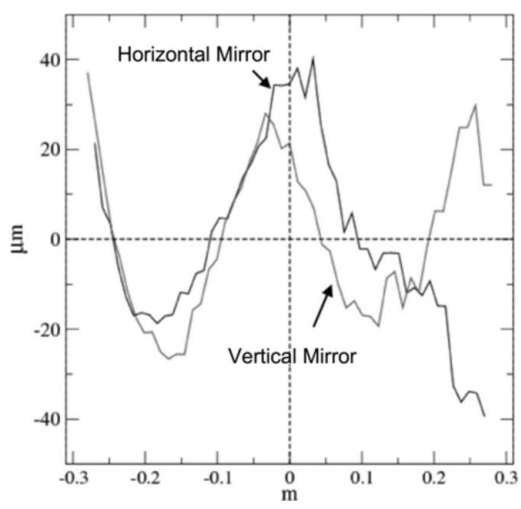

Figure 6
Estimated deflection of the beam from the ideal focal spot as a function of position along the mirror.

3. Actual mirror performance on SNAP

The mirrors were installed on the SNAP beamline and the neutron performance was compared with the predicted performance based on the LTP measurements. After the mirrors had been physically installed on the beamline, the beam just upstream of the mirrors was limited by a slit system with boron nitride blades. This aperture was set near the 2.4 × 2.4 mm projection of the ~0.6 m-long mirrors at a glancing angle of ~4 mrad. The object was a computer-controlled boron nitride slit ~6.49 m upstream of the mirrors.

The integrated flux in the focused beam was estimated at about 50% of the unfocused flux before the mirrors. This is consistent with a lower than unit reflectivity of the mirrors – especially at short wavelengths – and with the small ~200 μm gap between the mirror surfaces. This gap is unavoidable with mirrors that have straight edges.

The mirror angles were roughly calibrated by observing the direct, singly reflected and doubly reflected beams on a real-time neutron-sensitive area detector ~0.5 m behind the sample position (image plane). A double peak was observed in the doubly deflected beam. This peak structure is a consequence of the small gap between the two mirrors. At the intersection of the two mirrors, the side deflecting mirror should have an elliptically profiled edge so it can match the curvature of the other mirror. The estimated gap ranges from a few tens of μm at the ends (not quite touching) to about 200 μm in the center of the mirror system. Because this gap

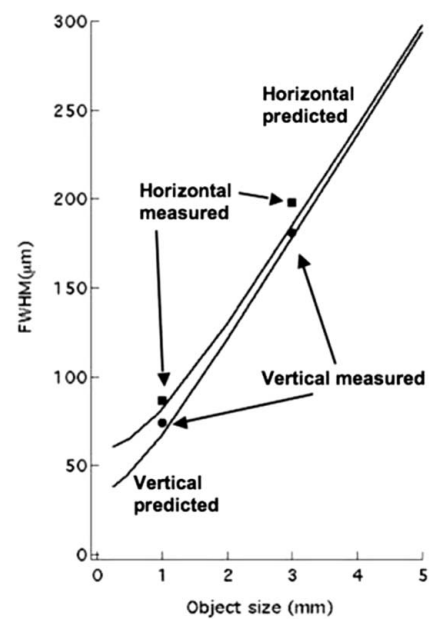

Figure 7
Spot size as a function of object size. The beam size at the sample can be easily tuned by the size of the object slit. The spot size can also be adjusted independently in each direction to maximize the signal at an asymmetrically shaped sample.

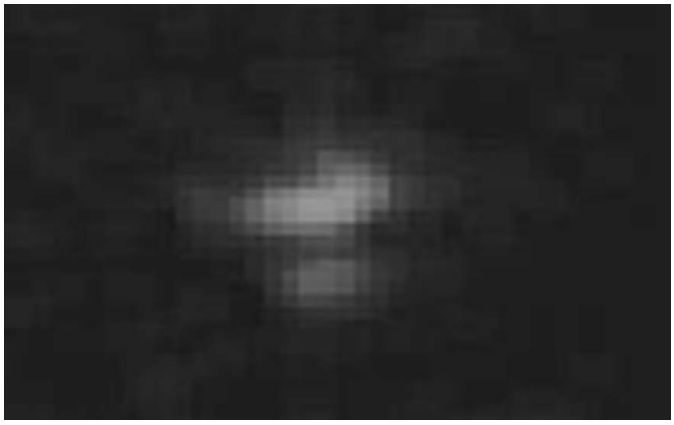

Figure 8
Typical reflection from a sample in a pressure cell. The structure in the peak is real and arises from the gap between the two mirrors. This gap can be eliminated by shaping the mirror edge to nest against its partner mirror surface.

affects only the vertical focusing mirror, the ~20% losses are observed as a horizontal stripe in the far field and in the diffraction spots (Fig. 8). No dispersion was measurable in the focused beam. Efforts are now underway to adjust the beamline software to account for the doubly deflected incident beam and to include the theoretical divergence structure into the peak fitting and data analysis.

4. Conclusions

Nested or Montel supermirror optics that collect about 2.6 times the divergence of sequential KB mirrors have been used to produce a polychromatic ~75 × 75 μm beam on the SNS SNAP beamline. The beam intensity is suitable for structure determination on samples ranging from ~75 to 500 μm. The slightly complicated divergence distribution can be removed by profiling the edge of one mirror. The approach described here can in principle be introduced into any neutron beamline to maximize signal-to-noise and signal for small (<1000 μm) samples.

This research was performed in part at the ILL, ESRF and SNS. The Spallation Neutron Source is managed by UT-Battelle, LLC, under contract No. DE-AC05-00OR22725 for the US Department of Energy. GEI and JWLP are supported by the DOE, Division of Materials Sciences and Engineering, Office of Basic Energy Sciences. PZT is supported by the DOE, Nuclear and Particle Physics. CT and JM are supported by the DOE Division of Scientific Facilities. KHA and TB are supported by the Institut Laue–Langevin, France. JYC is supported by the Pohang Accelerator Laboratory, Republic of Korea.

References

Ice, G. E. (2007). *Nucl. Instrum. Methods Phys. Res. Sect. A*, **582**, 129–131.
Ice, G. E. (2008). *Metall. Mater. Trans. A*, **39**, 3058–3064.
Ice, G. E., Choi, J.-Y., Takacs, P. Z., Khounsary, A., Puzyrev, Y., Molaison, J. Ju., Tulk, C. A., Andersen, K. H. & Bigault, T. (2009). *Metall. Mater. Trans. A*. In the press.
Ice, G. E., Hubbard, C. R., Larson, B. C., Pang, J. W. L., Budai, J. D., Spooner, S. & Vogel, S. C. (2005). *Nucl. Instrum. Methods Phys. Res. Sect. A*, **539**, 312–320.
Ice, G. E., Hubbard, C. R., Larson, B. C., Pang, J. W. L., Budai, J. D., Spooner, S., Vogel, S. C., Rogge, R. B., Fox, J. H. & Donaberger, R. L. (2006). *Mater. Sci. Eng. A*, **437**, 120–125.
Kirkpatrick, P. & Baez, A. V. (1948). *J. Opt. Soc. Am.* **38**, 766–774.
Liu, W., Ice, G. E., Tischler, J. Z., Khounsary, A., Liu, C., Assoufid, L. & Macrander, A. T. (2005). *Rev. Sci. Instrum.* **76**, 113701.
Mimura, H., Yumoto, H., Matsuyama, S., Sano, Y., Yamamura, K., Mor, Y., Ybashi, M., Nishino, Y., Tamasaku, K., Ishikawa, T. & Yamuchi, K. (2007). *Appl. Phys. Lett.* **90**, 051903.
NanoTechWire.com (2009). *Spallation Neutron Source Sees First Target Replacement*, http://www.nanotechwire.com/news.asp?nid=8293.
Puzyrev, Y. S., Ice, G. E. & Takacs, P. Z. (2009). *Nucl. Instrum. Methods Phys. Res. Sect. A*, **598**, 515–517.
SwissNeutronics (2009). *Concept of Neutron Mirrors/Supermirrors*, http://www.swissneutronics.ch/products/concept-supermirrors.html.
Yang, W., Larson, B. C., Ice, G. E., Tischler, J. Z., Budai, J. D. & Chung, K.-S. (2003). *Appl. Phys. Lett.* **82**, 3856–3858.